AIAA JOURNAL
Vol. 30, No. 8, August 1992

Two-Stream, Supersonic, Wake Flowfield Behind a Thick Base, Part I: General Features

V. A. Amatucci*
Sandia National Laboratories, Albuquerque, New Mexico 87185
J. C. Dutton†
University of Illinois at Urbana-Champaign, Urbana, Illinois 61801
D. W. Kuntz‡
Sandia National Laboratories, Albuquerque, New Mexico 87185
and
A. L. Addy§
University of Illinois at Urbana-Champaign, Urbana, Illinois 61801

An experimental investigation of the complex interaction region generated by the separation of two supersonic streams past a finite-thickness base has been conducted in a two-dimensional wind tunnel. The data were obtained using schlieren photography, pressure measurements, and two-component laser Doppler velocimeter measurements. The shear-layer mixing regions are characterized by initially constant-pressure mixing, by an evolution of velocity profiles from truncated boundary-layer shapes to wakelike profiles farther downstream, and by relatively high levels of turbulence. The separated flow region is characterized by large reverse flow velocities and strong interactions with the low-velocity regions of both shear layers. Turbulence intensities and kinematic Reynolds stresses are strongly affected by the separation process at the base and increase greatly in the latter portions of the two shear layers and in the recompression region. Recovery of the mean velocity field in the redeveloping wake occurs quickly, while the turbulence field remains perturbed to the furthest streamwise location investigated.

Nomenclature

C_f = skin-friction coefficient
H = splitter plate height, 25.4 mm
k = turbulent kinetic energy
M = Mach number
O = origin location for the coordinate system
P = pressure
Re = Reynolds number
Re_δ = Reynolds number based on boundary-layer thickness
Re_θ = Reynolds number based on momentum thickness
u = U-component of the velocity vector
u_τ = friction velocity
v = V-component of the velocity vector
w = width of the wind tunnel test section
X = coordinate parallel to the wind tunnel floor
Y = coordinate perpendicular to the wind tunnel floor
Z = spanwise coordinate
δ = boundary-layer thickness
δ^* = boundary-layer displacement thickness
θ = boundary-layer momentum thickness
λ = wavelength of laser light
ν = kinematic viscosity
Π = wake strength parameter
τ = shear stress
$\langle\ \rangle$ = root-mean-square quantity

Subscripts

Base = condition immediately behind the splitter plate
e = edge condition
J = inner jet or lower stream condition
w = condition at the wall
1 = condition for the Mach 2.56 stream (upper stream)
2 = condition for the Mach 2.05 stream (lower stream)
∞ = infinity or freestream conditions of the Mach 2.56 stream

Superscripts

$\overline{\ }$ = ensemble average
$'$ = fluctuation from the mean value

Introduction

THE complex interaction region generated by the separation of two supersonic streams past a finite-thickness base occurs frequently in high-speed flight and is characteristic of the aft-end flowfield of a powered missile in the supersonic flight regime. This fluid dynamic flowfield exists in other applications as well, including the flow region at the trailing edge of a blunt airfoil in a supersonic freestream or the initial mixing region of confluent multiple streams in a supersonic combustor. In each of these cases the near-wake region is dominated by strong velocity and density gradients, energetic viscous interactions, and expansion and compression processes covering the full range of gas dynamic regimes.

Research programs through the years have attempted to develop analytical, numerical, and experimental insight into the fluid dynamic processes ongoing in the near-wake region. The usual motivating goal is the development of a predictive capability for base pressure and other flowfield properties over a wide range of flight regimes. The analyses develop a physical flow model of the strong dissipative regions of the

Presented in part as Paper 90-0707 at the AIAA 28th Aerospace Sciences Meeting, Reno, NV, Jan. 8–11, 1990; received Jan. 2, 1991; revision received Nov. 22, 1991; accepted for publication Nov. 25, 1991.

*Senior Member of Technical Staff, Thermophysics Department. Member AIAA.
†Professor, Department of Mechanical and Industrial Engineering. Associate Fellow AIAA.
‡Senior Member of Technical Staff, Thermophysics Department. Senior Member AIAA.
§Professor and Head, Department of Mechanical and Industrial Engineering. Associate Fellow AIAA.

near wake, including interaction with the adjacent inviscid regions, and attempt to find applicability for a variety of Mach number, Reynolds number, and afterbody geometry conditions. The dominant analytical approach has been the Chapman-Korst component model[1,2] in which the turbulent base flowfield is separated into distinct regions and each part is analyzed individually, subject to appropriate assumptions and boundary conditions. The expansion process at the geometric corner, the shear layer mixing process, and the recompression and redevelopment processes (see Fig. 1) are each analyzed as separate components, utilizing empirical formulations as needed. The individual components are then joined together into an overall model of the separated flowfield, allowing for interaction between each component, and a unique solution is determined.

With the advent of more powerful computing facilities during recent years, both thin-layer and full Navier-Stokes computations of high-speed separated base flows have been performed. To date the agreement of these computations with experimental measurements of high-speed separated flowfields has been only moderate.[3] However, by focusing on the issues of grid resolution and alignment, as well as turbulence modeling, improved predictions of these flows have recently been obtained.[4-8] The difficulty in accurately computing these flows is understandable due to their complexity, since they include regions of large flow property gradients in thin shear layers, expansion waves, and shock waves, and also due to the inability of the current generation of turbulence models to adequately treat such effects as large streamline curvature, compressibility (i.e., high Mach-number effects), shear-layer impingement, and the effects on turbulence of the previously mentioned large gradient regions.

To aid in the understanding of the detailed mechanisms of these high-speed flows both with and without regions of significant flow separation, a program of small-scale wind tunnel experiments of simple flow geometries has been conducted at the University of Illinois at Urbana-Champaign. Initial experimental work has examined in detail the shear-layer mixing process[9,10] and the recompression and reattachment processes.[11-13] The measurements presented here take the next step in this progression and add the recirculating region and the wake redevelopment region (see Fig. 1) as focuses of study to obtain experimental data for a unified two-stream near-wake flowfield. The present experimental program has

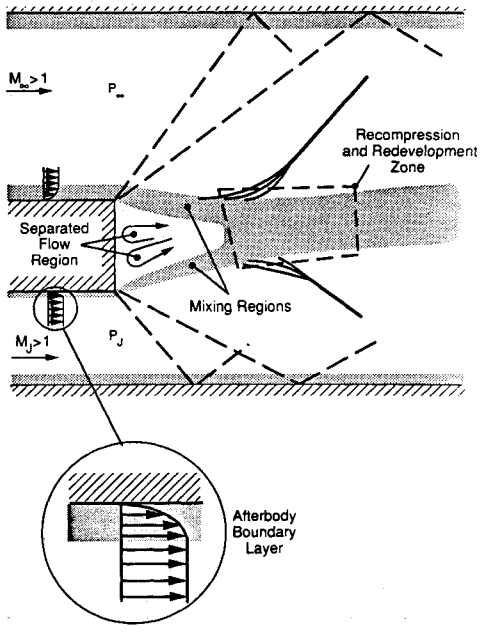

Fig. 1 Detailed flowfield characteristics generated by the separation of two supersonic streams past a finite-thickness base.

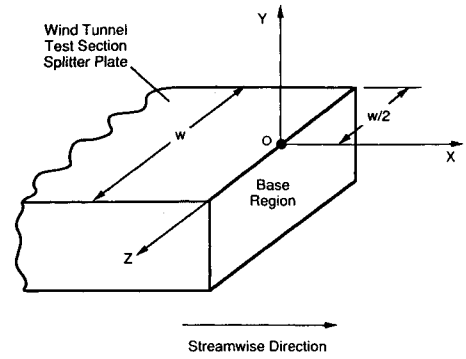

Fig. 2 Schematic of the origin location and coordinate system used for collection and presentation of the near-wake interaction mean and turbulence data.

obtained measurements over the full range of mechanisms exhibited in this flowfield for a well-determined set of incoming flow conditions. The data for these experiments are obtained from schlieren photography, sidewall pressure measurements, and laser Doppler velocimeter (LDV) measurements. The use of a two-color, two-component, frequency-shifted LDV system to measure instantaneous flow velocity, despite its added complexity, has certain special advantages in the near-wake separated flowfield. Most past near-wake interaction experiments have focused on mean velocity values obtained from pressure distribution data gathered by intrusion into the near wake, usually with a single pressure probe or a probe rake. The LDV measurements of the current investigation provide accurate instantaneous velocity data obtained in a nonintrusive way by an instrument requiring no prior calibration.

The primary objective of this experimental investigation of the supersonic, two-stream base flow is to investigate the fundamental fluid dynamic mechanisms existing in the near-wake flowfield with an aim toward better understanding of each individual process and how they interact. Detailed data have been collected in all regions of the near-wake flowfield in order to examine such features as changes in velocity profiles due to the corner expansion process, evolution of the velocity profiles during shear-layer mixing, strength and influence of the recirculating region, and mean and turbulent flowfield changes during the recompression, reattachment, and downstream wake redevelopment processes.

The results and trends of the LDV data obtained for the two-stream interaction flowfield are presented in a series of two articles. This first article presents the background, objectives, and techniques involved in making the velocity measurements in this flowfield, and then gives general trends and features of the mean and turbulence fields for the overall global interaction as they change with downstream distance. In the second paper, detailed data will be shown for each of the *components* of the flowfield, such as the shear-layer mixing regions and the recompression/reattachment region, and trends for each component will be compared to literature specific for that component. The two papers, taken together, will then form a complete picture of the turbulent nature of this near-wake interaction.

Experimental Facilities and Measurement Techniques

Facilities

This investigation of the near-wake interaction utilized the air supply and wind tunnel facilities of the Mechanical Engineering Laboratory at the University of Illinois at Urbana-Champaign for a series of dry, cold air experiments. A two-dimensional wind tunnel test section, shown schematically in Fig. 1, produced two uniform supersonic streams which separated at the geometric corners of a finite-thickness splitter

plate and formed a flowfield characteristic of the aft-end of a powered missile, including expansion at the separation points, formation of a recirculating region bounded by two shear-layer mixing regions, recompression and reattachment of the shear layers, and downstream wake redevelopment.

The common upstream plenum chamber provided compressed air at 517 kPa to two separate pipe-and-valve arrangements supplying the two converging-diverging nozzles. These nozzles used the splitter plate as a half-nozzle symmetry plane. The upper stream nozzle produced a uniform exit plane flow 50.8 mm in height, having a Mach number of 2.56, and a splitter plate boundary-layer thickness of 3.35 mm. The lower stream nozzle was shorter in length and produced a uniform exit plane flow 25.4 mm in height, having a Mach number of 2.05, and a splitter plate boundary-layer thickness of 1.46 mm. These two supersonic streams separated past the 25.4-mm-thick base and produced the near-wake interaction flowfield. The test section region was 50.8 mm wide and 101.6 mm in height and was within view of clear glass windows on both sides of the wind tunnel for optical diagnostic access. As illustrated in Fig. 2, the origin for the coordinate system was located on the centerline of the wind tunnel at the upper rear edge of the splitter plate. All features of the near-wake flowfield, including wake redevelopment, occurred within the measurement domain before the mixed flow exited the test section through a constant-area diffuser.

Measurement Techniques

The measurement techniques employed in this investigation included schlieren photography, stagnation and static pressure measurements, and laser Doppler velocimetry. Schlieren photographs obtained with a 1.4-μs spark source were used to characterize the qualitative features of the overall flowfield and to determine spatial locations for LDV measurements. The sidewall static pressure data were collected using an aluminum window insert which replaced one of the glass side windows and had a grid of 370 pressure taps. The pressure levels were measured with a Pressure Systems Incorporated (PSI) digital pressure transmitter system and yielded pressure measurements in all regions of the near-wake interaction including along the shear-layer mixing regions.

The two-component, two-color LDV system was based on Thermal Systems Incorporated (TSI) optical and electronic components and employed a Spectra-Physics 5-W argon ion laser. The green beam ($\lambda = 514.5$ nm) and the most powerful blue beam ($\lambda = 488.0$ nm) were used in the beam splitting and recombination processes which produced the ellipsoidal measurement volumes. The use of a 350-mm focal length transmitting lens with 22-mm beam spacing produced a green measurement volume of 0.183 mm diameter, 6.08 mm length, with 8.53-μm fringe spacing. The blue measurement volume diameter, length, and fringe spacing were 0.179 mm, 5.92 mm, and 8.09 μm, respectively. These fringe spacings, in combination with the 40 MHz frequency shift and orientation of the fringes at ± 45 deg to the mean flow direction, kept signal frequencies within range of the electronic equipment while moving the fringes at a high enough velocity to reduce fringe bias probabilities and eliminate directional ambiguity. TSI frequency counters, operated in the single-measurement-per-burst mode with high- and low-pass filtering, were used to determine the Doppler shift frequencies of the signals from the photodetectors and to perform validation checks to remove erroneous data. The receiving optics of the LDV system were oriented in a forward scatter mode 10 deg from the optical axis in order to reduce the effective length of the measurement volume to 1.46 mm and to provide optimum signal-to-noise ratio of the scattered laser light. The output from the LDV system's frequency counters was stored in the memory of a DEC PDP 11/73 minicomputer by means of a direct memory access board, and the data were transferred serially to an HP-9000 computer system for reduction, analysis, and plotting. The laser, transmitting optics, and collection optics were mounted on a traversing table which allowed movement in all three coordinate directions with an accuracy of approximately ± 0.1 mm.

Seeding of the flow for the LDV measurements was accomplished by injecting silicone oil droplets (50 cP viscosity) produced by a TSI six-jet atomizer into the stagnation chamber. To address the issues of particle size and flow-following capability (i.e., particle dynamics effects), a series of particle lag experiments was conducted whereby LDV measurements were made across an oblique shock wave produced by a 15-deg compression corner in a Mach 2.0 wind tunnel. Using these measurements, together with a particle relaxation analysis based on the work of Maxwell and Seasholtz[14] and the drag law of Walsh,[15] the silicone oil droplets used in these experiments are estimated to be 1.0 μm in diameter. Droplets of this size have an Eulerian frame of reference frequency response of up to approximately 200 kHz which is adequate for following the turbulent fluctuations of the current near-wake flowfield.

The use of counter-type signal processors to measure individual velocity realizations introduces additional considerations, especially in high-speed flows, due to counter clock resolution, statistical uncertainty, velocity bias, fringe bias, and spatial resolution. The ± 1 ns accuracy of the counters results in a minimum measurable turbulence intensity in the highest speed regions of the flow of 1.37%, with proportionately smaller values in the lower speed regions. To control the uncertainty due to finite sample size, either 2048 or 4096 velocity realizations were generally collected throughout the flowfield. At a confidence level of 95%, the resulting statistical uncertainty in the mean velocity is therefore a maximum of $\pm 3\%$ for turbulence intensities less than about 100%, and the statistical uncertainty in the standard deviation is a maximum of approximately $\pm 3.1\%$. For the current low data density measurements,[16] the seed particles generated valid Doppler signals at a rate several orders of magnitude lower than the capability of the processors to sample, resulting in a free running processor condition in which the LDV data is totally velocity biased.[10] To correct for this condition, a two-dimensional inverse velocity magnitude weighting scheme[17] has been employed. As mentioned, the relatively large fringe spacing, use of the 40-MHz frequency shift, and the ± 45-deg orientation of the fringes to the mean flow direction, greatly reduced the possibility of fringe bias in these experiments. In fact, an implementation of the fringe bias analysis of Buchhave[18] demonstrated that for the vast majority of the measurements the fringe bias correction was less than 3% and, as a result, no such correction has been used in the measurements presented here. Spatial-resolution errors can also occur in high-gradient regions of the flow due to the finite size of the probe volume. Using the analysis of Karpuk and Tiederman,[19] the maximum spatial-resolution error at the location 5 mm downstream

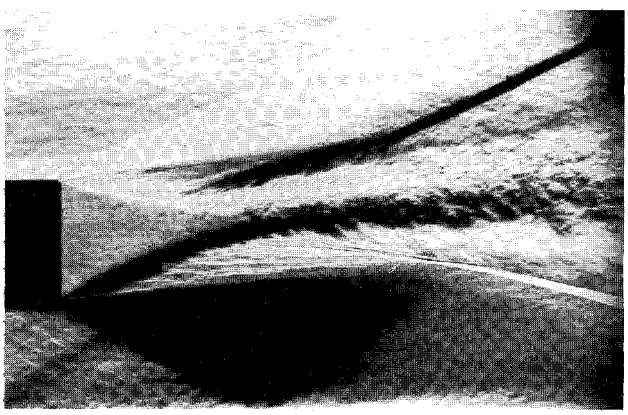

Fig. 3 Schlieren photograph of the two-stream interaction flowfield visible through the sidewall windows of the wind tunnel test section (1.4-μs flash duration).

Table 1 Properties of the Mach 2.56 and Mach 2.05 boundary layers

Parameter	Upper stream	Lower stream
Mach number	2.56	2.05
δ, mm	3.35	1.46
δ^*, mm	0.947	0.393
θ, mm	0.220	0.118
Re, m^{-1}	5.12×10^7	6.36×10^7
Re_θ	1.12×10^4	7.48×10^3
Π	0.9216	1.121
u_τ, m/s	25.11	21.45
C_f	0.001597	0.001821

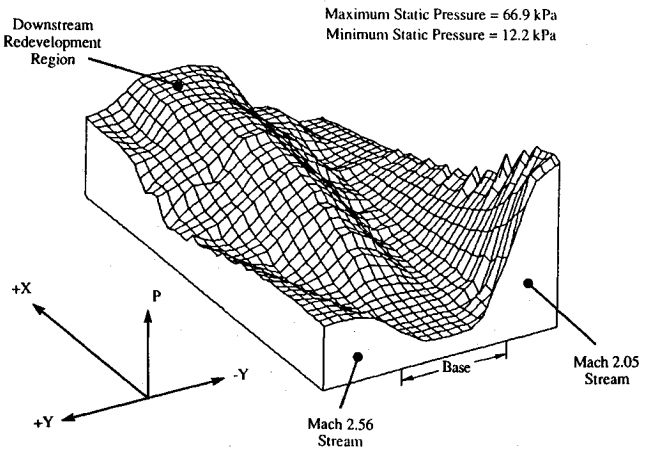

Fig. 4 Three-dimensional surface contour representation of the static pressure levels existing in the near-wake interaction flowfield (viewed from upstream).

from the base is estimated to be ± 2.8% for the mean velocity and ± 4.8% for the turbulence intensity, with much smaller errors in the downstream regions of the near-wake flow.

Further details concerning the equipment and apparatus, measurement methods, and experimental procedures are found in Ref. 20.

Experimental Results and Discussion

Two-Dimensionality of the Flowfield

Past work[21,22] has indicated the tendency for existence of spanwise nonuniformity in flowfields characterized by large embedded separation regions leading to reattachment. To examine these effects in the present flowfield, transverse profiles of velocity were obtained at three spanwise locations: at the midplane ($Z = 0$) and at $Z = \pm 10$ mm from the midplane. In addition, these profiles were obtained at three *streamwise* locations chosen to examine distinctly different regions of the near-wake flowfield: $X = 25$ mm where separate shear layers and recirculation were present, $X = 45$ mm in the recompression and reattachment region, and $X = 100$ mm in the redeveloping downstream wake. The centerline and off-centerline streamwise mean velocity and turbulence intensity profiles show that the central 40% of the test section flowfield was highly two-dimensional in all regions, with the largest deviations occurring in the recirculating region. Once impingement of the two shear layers occurred, the LDV data indicate very little deviation from two-dimensionality at any transverse location. Although regions of slight three-dimensionality do exist, they seem characteristic of the fluid dynamic processes ongoing in those components of the near-wake and are not due to the wind tunnel design or sidewall boundary layers.

Turbulent Boundary Layers

The turbulent boundary-layer characteristics of the two supersonic streams provide the initial conditions for the expansion, mixing, recompression, and redevelopment processes which occur in the near wake. Detailed LDV measurements were made of the boundary layers which developed on the upper and lower surfaces of the splitter plate at a location 4 mm before geometric separation. Two-component measurements were made to a distance of 0.75 mm from either surface and then one-component measurements completed the survey to a distance within 0.25 mm above either surface. The measured velocity profiles for the upper and lower boundary layers were fit to the generalized velocity profile equation of Sun and Childs[23] using the boundary-layer thickness δ, the friction velocity u_τ, and the wake strength parameter Π as curve-fit coefficients. The important parameters describing the growth and development of the two boundary layers prior to separation are presented in Table 1. The differences in thicknesses between the Mach 2.56 stream ($\delta = 3.35$ mm) and the Mach 2.05 stream ($\delta = 1.46$ mm) were generated intentionally to simulate the ratio of boundary-layer thicknesses typical of powered missile applications. The aim was to simulate zero angle-of-attack configurations while including the effects of strong expansion of the inner propulsive flow. The wake strength parameter, friction velocity, and skin-friction coefficient values are consistent with earlier studies[9,11-13,21,24,25] of compressible turbulent boundary layers.

Global Near-Wake Interaction Flowfield

Schlieren photography has been used to obtain a qualitative view of the component processes existing in the near-wake interaction. The schlieren photograph of Fig. 3 shows well-developed splitter plate boundary layers undergoing strong expansion and turning processes at geometric separation. The two free shear layers generated at separation appear to be initially very thin and to undergo a moderately long constant pressure mixing region before they show any signs of curvature associated with the recompression process prior to impingement. The beginning of the recompression process for each shear layer is marked by the first compression waves which emanate from the slightly supersonic regions of the shear layer and eventually coalesce into the recompression oblique shock wave. One of the more interesting features in this photograph is the apparent large-scale turbulent structures which border the edges of the redevelopment core produced by the impingement of the two free shear layers. These structures are similar to those that occur in high-Reynolds-number free jets and have an effect on the turbulence intensities measured in the redeveloping wake. Similarly, each shear layer shows signs of large-scale structures and intermittency at its edges, especially on the side bounded by the recirculating region.

The arrangement of sidewall static pressure tap locations was designed to obtain detailed pressure surveys of the expansion process, mixing layers, and recompression and redevelop-

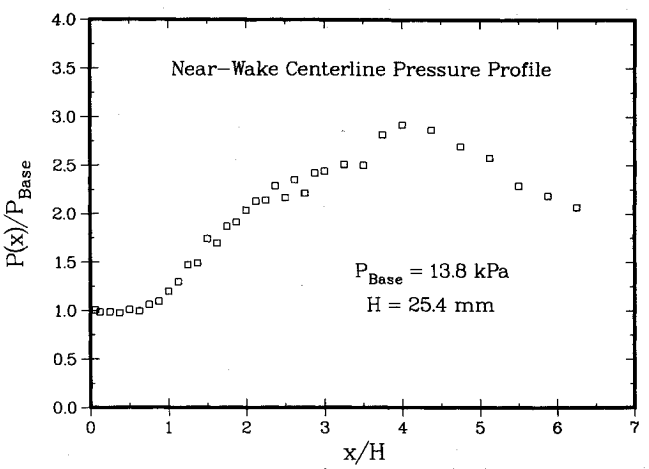

Fig. 5 Centerline pressure profile ($Y/H = -0.5$, $Z = 0$, X variable) for the near-wake interaction region.

ment processes. The three-dimensional contour plot of Fig. 4 shows the static pressure data viewed by an observer located upstream at the base and looking in the streamwise direction. Although no detailed vertical scale is given for the levels of static pressure, a relative indication of the pressure magnitude can be obtained by recognizing that the maximum static pressure in the figure is 66.9 kPa and occurs at the exit of the Mach 2.05 nozzle, while the minimum static pressure of 12.2 kPa occurs in the highly expanded flow region downstream of the Mach 2.05 nozzle and just upstream of the lower recompression shock wave. In a quantitative sense the plot of Fig. 4 shows the strong expansion of the two supersonic streams to the low base pressure "valley" immediately behind the finite-thickness base, the initially constant pressure mixing of the two shear layers, and the gradual but strong pressure rise through the recompression and reattachment regions extending into the downstream wake redevelopment region. The base pressure measured in the region behind the splitter plate was 13.8 kPa.

A profile of the measured static pressure along a centerline extending downstream from the vertical center of the splitter plate is shown in Fig. 5. The static pressure has been nondimensionalized by the average base pressure (13.8 kPa) and the streamwise distance was nondimensionalized by the value of the splitter plate height. The data in Fig. 5 indicate the relatively constant pressure existing in the recirculating region just downstream of the base and the strong pressure rise which occurs during the recompression and impingement process for the two shear layers. Since impingement of the shear layers occurs at approximately $X/H = 1.37$, the data illustrate the initial pressure rise up to reattachment and the substantial increase in pressure existing downstream of that location. The maximum pressure rise level of $P/P_{Base} = 2.92$ (at $X/H = 4.0$) is consistent with other experimental data[11-13] and indicates the strong mixing and diffusionlike processes occurring in the separated flow region.

The LDV data presented in this paper are intended to give an overview of the mechanisms existing in the near-wake interaction, including a detailed indication of the mean flow and some turbulence quantities. The objective of this overview is to show representative data highlighting the dramatic changes in mean velocity and turbulence quantities in the region immediately behind the splitter plate and in the initial stages of recompression and reattachment. The LDV data presented herein include the "reference" upstream boundary-layer traverses, *every other* vertical traverse from 5.0 mm behind the splitter plate to 40.0 mm downstream, and then *every* measured traverse from $X = 40.0$ to 55.0 mm. In the case of the data presented in Fig. 12, the profiles extend to the farthest downstream location, namely at $X = 160$ mm. The omission of some LDV traverses from the figures for the global interaction was necessary to reduce plot congestion. In the presentation of these results, all of the instantaneous velocity data obtained with the LDV system have been rotated to a coordinate system which aligns the u-component direction parallel to the wind tunnel floor (primary streamwise direction) and the v-component direction perpendicular to the wind-tunnel floor (see Fig. 2).

The mean velocity profiles obtained from the LDV instantaneous data are shown in vector representation in Fig. 6. The vector field plot clearly shows the approach and separation of the two turbulent boundary layers from the upper and lower surfaces of the splitter plate, with the resulting large separated flow region. The shear-layer mixing regions spread with streamwise distance until impingement occurs approximately 1.4 base heights downstream of separation (at $X = 34.9$ mm), where the recirculating region ends (no negative streamwise velocity components are measured) and recovery of the wake

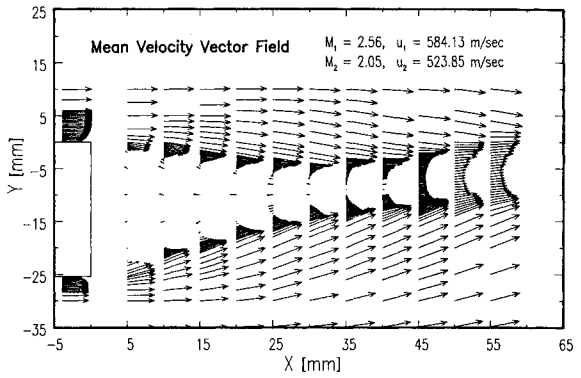

Fig. 6 Mean velocity vector field for the two-stream interaction flowfield showing the near-wake region.

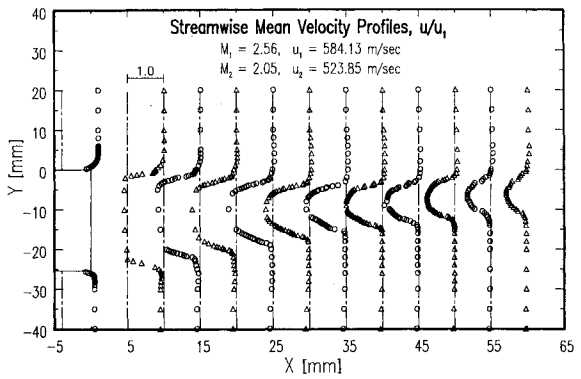

Fig. 7 Streamwise mean velocity profiles for the two-stream interaction flowfield showing the near-wake region.

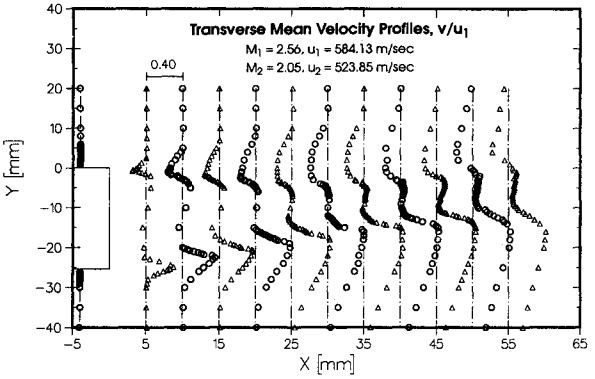

Fig. 8 Transverse mean velocity profiles for the two-stream interaction flowfield showing the near-wake region.

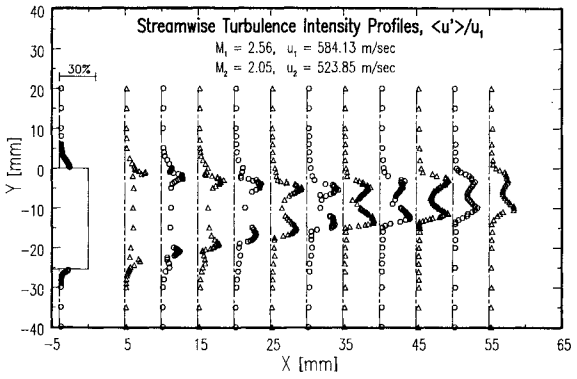

Fig. 9 Streamwise turbulence intensity profiles for the two-stream interaction flowfield showing the near-wake region.

deficit begins. The turbulent mixing which occurs throughout the recompression and reattachment regions quickly effects elimination of the velocity deficit by approximately five base heights downstream of separation, although only part of this process can be seen in Fig. 6.

Examining Fig. 6 in greater detail, the data show that the upper Mach 2.56 flow has a freestream velocity of 584 m/s before separation and expands sharply downward around the corner of the base to a flow angle of approximately -10.6 deg (relative to the freestream). The lower Mach 2.05 freestream moves at a velocity of 524 m/s before separation and then expands upward about the splitter plate corner at an angle of approximately 21.6 deg. Both turbulent boundary layers are fully developed and expand upon geometric separation to a matched base pressure of 13.8 kPa which exists in the recirculating region. The inner jet-to-freestream static pressure ratio (P_J/P_∞ or P_2/P_1) just prior to geometric separation was measured to be 2.14. The mean velocity vectors shown in Fig. 6 illustrate the complex nature of separation past a relatively thick base, and indicate differences from the type of wake developed behind a very thin splitter plate.[26]

The vector representation of the recirculating region in Fig. 6 indicates the existence of two large separation bubbles. The upper separation bubble rotates clockwise while the lower bubble rotates counterclockwise, and relatively large velocity magnitudes exist in this region. Historically posed by Korst[2] as a "dead-air" region, the recirculating region of the near-wake in the present investigation had a maximum negative velocity of 132 m/s at the $X = 22.5$ mm streamwise location. This maximum reverse flow velocity magnitude of $0.23u_1$ is very consistent with the results of Petrie et al.,[9,10] Samimy et al.,[11-13] and Etheridge and Kemp,[27] in the entire range of Mach numbers.

The streamwise mean velocity profiles, nondimensionalized by the edge velocity of the Mach 2.56 stream prior to separation, are shown in Fig. 7. The dashed line at each X value represents the streamwise location of the traverse and the $u/u_1 = 0$ plane for that set of data. The upstream boundary-layer profiles represent a typical range of u/u_1 beginning at a value of 1.0 in the Mach 2.56 stream and 0.90 in the Mach 2.05 stream ($u_2/u_1 = 0.9$) and decreasing to zero on the two surfaces of the splitter plate. This series of profiles once again indicates the large negative velocities occurring in the recirculating region and the recovery of the velocity defect with downstream distance. The very fine transverse resolution of the LDV measurement locations yields u-component data which show the spreading of the velocity profiles in each of the shear layers from a very sharp gradient at the $X = 5.0$ mm location to a much broader velocity change for the thickened shear layers at the streamwise stations near recompression and reattachment. The rapid recovery of the mean velocity defect is consistent with the data of Samimy and Addy[13] for a similar two-stream near-wake interaction between Mach 2.07 and Mach 1.50 streams.

The mean velocity field in the transverse direction is shown in Fig. 8 for the range of profiles in the near-wake region. The sign convention illustrated by the data is consistent with the coordinate system defined using Fig. 2; the large positive values of v/u_1 occurring for the lower stream indicate the strong expansion and turning which that region experiences during the mixing process. One noticeable difference between the streamwise and transverse mean velocity profile characteristics for any particular X location is the slower relaxation of the transverse profiles with downstream distance.

The turbulence field, represented in part by the streamwise turbulence intensity profiles of Fig. 9, demonstrates strong enhancement of mixing due to the interaction at the base. The counter clock resolution problem with the LDV system is illustrated in the edge values of $\langle u' \rangle/u_1$ of approximately 2% in the two relatively high-velocity isentropic core flows. The

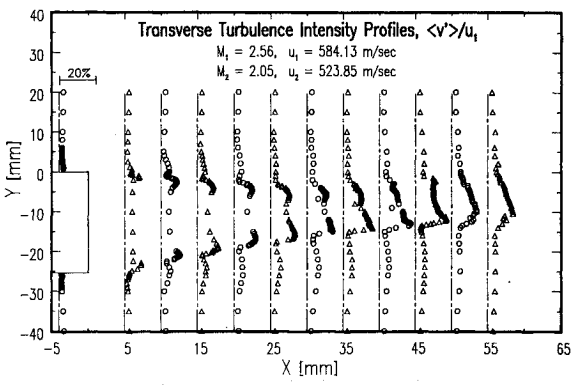

Fig. 10 Transverse turbulence intensity profiles for the two-stream interaction flowfield showing the near-wake region.

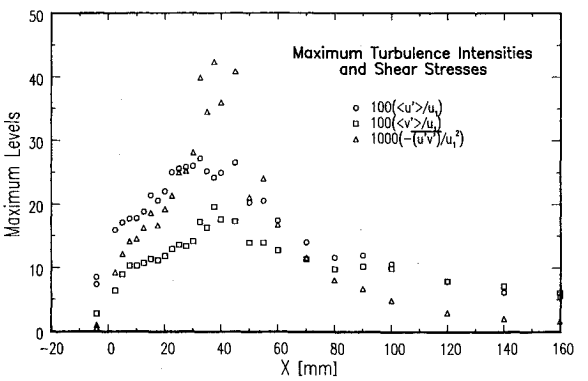

Fig. 12 Maximum turbulence intensities and shear stresses for the two-stream interaction flowfield showing the entire streamwise range of measurements.

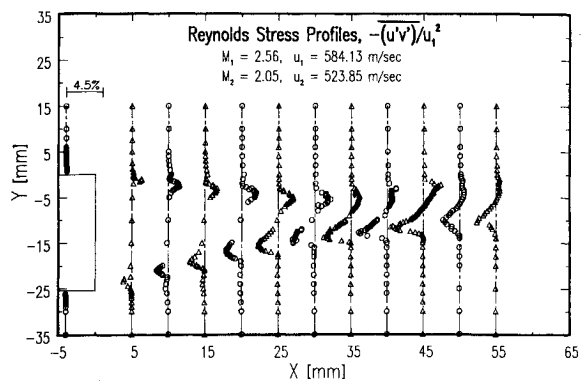

Fig. 11 Kinematic Reynolds stress profiles for the two-stream interaction flowfield showing the near-wake region.

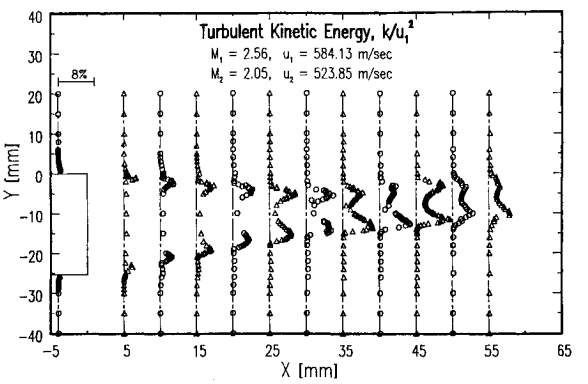

Fig. 13 Turbulent kinetic energy profiles for the two-stream interaction flowfield showing the near-wake region.

striking feature of Fig. 9, however, is the relatively high levels of streamwise turbulence intensity reaching nearly 30% in the latter streamwise stations in the mixing layers and in the recompression and reattachment regions. Despite similarities in the form of the turbulence intensity profiles across either shear layer to those found by Andreopoulos and Bradshaw[28] in an incompressible shear layer behind a flat plate and by Ikawa and Kubota[29] in a supersonic free shear layer, the levels of $\langle u' \rangle / u_1$ are dramatically higher in the present investigation. Although Samimy and Addy's[13] streamwise turbulence intensity levels were slightly lower than those shown in Fig. 9, the trends are similar and indicate strong shear-layer mixing and the highly turbulent nature of the reattachment process.

The transverse turbulence intensity profiles shown in Fig. 10 similarly reflect the strong mixing near recompression and the disturbed nature of the turbulence field even downstream to the last traverse location shown. Fig. 10, now scaled twice as sensitive for a maximum $\langle v' \rangle / u_1$ value of 30% (as compared to the scaling of $\langle u' \rangle / u_1$ in Fig. 9), shows the moderately low levels of transverse turbulence intensity existing in both of the upstream boundary layers in contrast to the high levels of $\langle v' \rangle / u_1$ occurring in the shear layers. The transverse turbulence intensity appears to spread more broadly across the transverse height of the interaction region than the streamwise turbulence intensity does and is similar to results obtained by Kuntz et al.[21] for a Mach 2.94 shock-wave/boundary-layer interaction flowfield.

The data for the kinematic Reynolds stress portion of the turbulent shear stress for the near-wake interaction region are nondimensionalized by the square of the Mach 2.56 edge velocity and plotted in Fig. 11. Initially low levels of Reynolds stress in the splitter plate boundary layers rise to relatively high levels immediately downstream of separation, persist throughout the mixing layer development, and reach maximum values in the recompression and reattachment regions. The Reynolds stresses then tend to decrease sharply after reattachment, very similar to the trends of incompressible reattachment as shown by the data of Chandrsuda and Bradshaw.[30] The lower Mach 2.05 stream's mixing layer appears to be more highly turbulent than the Mach 2.56 stream, and as suggested by Samimy and Addy[13] may be the result of a stronger separation and expansion process for this shear layer, or may be the consequence of a lower convective Mach number.[26] The decrease in Reynolds stress just downstream of reattachment has been explained by restriction of the larger eddies[30] and by bifurcation of the turbulent eddies at reattachment[31,32] resulting in much smaller length scales and lower Reynolds stresses.

The maximum levels of turbulence intensity and shear stresses in the near-wake interaction flowfield are plotted in Fig. 12 for each of the streamwise locations, including the traverses which were omitted previously (those in the range from $X = 2.5$ to 37.5 mm and the range from $X = 60$ to 160 mm). To fit all three quantities on the same ordinate, the streamwise and transverse turbulence intensities are shown in percent while the shear stress levels are actually 10 times the percent value. Since the reattachment of the two mixing layers into a single wake with no reverse velocities occurs at 34.9 mm behind the step, the maximum levels of the quantities plotted in Fig. 12 should peak in that region or slightly downstream. Both the streamwise turbulence intensity $\langle u' \rangle / u_1$ and the transverse turbulence intensity $\langle v' \rangle / u_1$ increase gradually from initially relatively low values in the boundary layers ($X = -4.0$ mm) to reach maximum levels in the general vicinity of reattachment, then decrease with increasing streamwise distance. The kinematic Reynolds stress, which indicates the correlation between the u' and v' fluctuations, tends to peak sharply in the reattachment region near the streamwise location of $X = 34.9$ mm, then decreases rapidly downstream.

The last data plotted for a global view of the near-wake interaction are the turbulent kinetic energy k nondimensionalized by the square of the Mach 2.56 stream edge velocity u_1. The three-dimensional turbulent kinetic energy, shown in Fig. 13, was obtained by estimating the w-component contribution to be an *average* of the streamwise and transverse variances. Since the turbulent kinetic energy tends to be dominated by the streamwise turbulence intensity, the value of k reaches its peak in the central regions of the mixing layers and maximizes in the recompression and reattachment regions. Research by Lee and Harsha[33,34] indicated that there existed a strong correlation between measurements of turbulent shear stress and turbulent kinetic energy in constant-density mixing flows, and extended to include typical wakelike flows. Their work determined that the shear stress levels were approximately three-tenths of the level of turbulent kinetic energy, with nearly 70% of the cases correlating with proportionality factors between 0.2 and 0.4. The decrease in turbulent kinetic energy with downstream distance in the redevelopment region and the diffusion of k outward with the growth of the redeveloping wake (shown in Fig. 13), when combined with the form of the decay in Reynolds stress as seen in Fig. 11, are trends which appear to verify that such that a correlation exists between those two quantities as observed by researchers[33-36] for wake flows and boundary-layer flows.

Conclusions

The near-wake interaction flowfield generated by the separation of two supersonic streams past a finite-thickness base is characterized by steep velocity gradients, high turbulence intensity levels, and viscous mixing in the presence of an adverse pressure gradient. The shear-layer mixing regions are characterized by constant-pressure mixing along the initial two-thirds of their length, and show an evolution of velocity profiles from truncated forms of the boundary-layer shapes to more wake-like profiles farther downstream. The region of separated flow existing between the two supersonic streams in the near-wake exhibits vigorous recirculation, maximum reverse flow velocity magnitudes reaching $0.23u_1$, and strong turbulent interaction with the low-velocity regions of both shear layers. Peak levels of turbulence intensity and Reynolds stress were measured in the recompression and reattachment regions and decreased rapidly with streamwise distance. The turbulence field in the region of recompression and reattachment is strongly anisotropic. LDV data for the redevelopment of the downstream wake flow showed lower levels of turbulence intensity and kinematic Reynolds stress than other regions of the near-wake interaction, but illustrated the strong preservation of the disturbed turbulence field with even large distances downstream. While recovery of the mean velocity profiles was achieved, much slower recovery of the turbulence field was seen.

Acknowledgments

The authors gratefully acknowledge the generous financial support of the U.S. Army Research Office under Contracts DAAL03-87-K-0010 and DAAL03-90-G-0021 with Thomas Doligalski as Contract Monitor. The authors also appreciate the efforts and assistance of Steven G. Goebel regarding generation of the three-dimensional contour plot of the sidewall static pressure data.

References

[1]Chapman, D. R., "An Analysis of Base Pressure at Supersonic Velocities and Comparison with Experiment," NACA TN 2137, July 1950.

[2]Korst, H. H., "A Theory for Base Pressures in Transonic and Supersonic Flow," *Journal of Applied Mechanics,* Vol. 23, No. 4, 1956, pp. 593-600.

[3]Petrie, H. L., and Walker, B. J., "Comparison of Experiment and Computation for a Missile Base Region Flowfield with a Centered Propulsive Jet," AIAA Paper 85-1618, July 1985.

[4]Venkatapathy, E., and Lombard, C. K., "Accurate Numerical Simulation of Jet Exhaust Flows with CSCM for Adaptive Overlapping Grids," AIAA Paper 87-0465, Jan. 1987.

[5]Sahu, J., "Computations of Supersonic Flow Over a Missile Afterbody Containing an Exhaust Jet," *Journal of Spacecraft,* Vol. 24, No. 5, 1987, pp. 403–410.

[6]Hoffman, J. J., Birch, S. F., and Hopcraft, R. G., "Navier-Stokes Calculations of Rocket Base Flows," AIAA Paper 87-0466, Jan. 1987.

[7]Childs, R. E., and Caruso, S. C., "On the Accuracy of Turbulent Base Flow Predictions," AIAA Paper 87-1439, Honolulu, HI, June 1987.

[8]Childs, R. E., and Caruso, S. C., "Assessment of Modeling and Discretization Accuracy for High Speed Afterbody Flows," AIAA Paper 89-0531, Reno, NV, Jan. 1989.

[9]Petrie, H. L., Samimy, M., and Addy, A. L., "Compressible Separated Flows," *AIAA Journal,* Vol. 24, No. 12, 1986, pp. 1971–1978.

[10]Petrie, H. L., Samimy, M., and Addy, A. L., "Laser Doppler Velocity Bias in Separated Turbulent Flows," *Experiments in Fluids,* Vol. 6, No. 2, 1988, pp. 80–88.

[11]Samimy, M., Petrie, H. L., and Addy, A. L., "A Study of Compressible Turbulent Reattaching Free Shear Layers," *AIAA Journal,* Vol. 24, No. 2, 1986, pp. 261–267.

[12]Samimy, M., Petrie, H. L., and Addy, A. L., "Reattachment and Redevelopment of Compressible Turbulent Free Shear Layers," *Proceedings of the ASME International Symposium on Laser Anemometry,* ASME FED-Vol. 33, Miami Beach, FL, Nov. 1985, pp. 159–166.

[13]Samimy, M., and Addy, A. L., "Interaction Between Two Compressible, Turbulent Free Shear Layers," *AIAA Journal,* Vol. 24, No. 12, 1986, pp. 1918–1923.

[14]Maxwell, B. R., and Seasholtz, R. G., "Velocity Lag of Solid Particles in Oscillating Gases and in Gases Passing Through Normal Shock Waves," NASA TN D-7490, March 1974.

[15]Walsh, M. J., "Influence of Particle Drag Coefficient on Particle Motion in High-Speed Flow with Typical Laser Velocimeter Applications," NASA TN D-8120, Feb. 1976.

[16]Edwards, R. V., "Report of the Special Panel on Statistical Particle Bias Problems in Laser Anemometry," *Transactions of the ASME: Journal of Fluids Engineering,* Vol. 109, Series I, No. 2, 1987, pp. 89–93.

[17]McLaughlin, D. K., and Tiederman, W. G., Jr., "Biasing Correction for Individual Realization of Laser Anemometer Measurements in Turbulent Flows," *Physics of Fluids,* Vol. 16, No. 12, 1973, pp. 2082–2088.

[18]Buchhave, P., "Biasing Errors in Individual Particle Measurements with the LDA-Counter Signal Processor," *Proceedings of the LDA-Symposium,* Copenhagen, Denmark, 1975, pp. 258–278.

[19]Karpuk, M. E., and Tiederman, W. G., Jr., "Effect of Finite-Size Probe Volume Upon Laser Doppler Anemometer Measurements," *AIAA Journal,* Vol. 14, No. 8, 1976, pp. 1099–1105.

[20]Amatucci, V. A., "An Experimental Investigation of the Two-Stream, Supersonic, Near-Wake Flowfield Behind a Finite-Thickness Base," Ph.D. Thesis, Dept. of Mechanical and Industrial Engineering, Univ. of Illinois at Urbana-Champaign, Urbana, IL, 1990.

[21]Kuntz, D. W., Amatucci, V. A., and Addy, A. L., "Turbulent Boundary-Layer Properties Downstream of the Shock-Wave/Boundary-Layer Interaction," *AIAA Journal,* Vol. 25, No. 5, 1987, pp. 668–675.

[22]Taghavi, K., "Unsteady Reattachment of Supersonic Flow Past a Backward-Facing Step," M.S. Thesis, Dept. of Mechanical and Industrial Engineering, Univ. of Illinois at Urbana-Champaign, Urbana, IL, 1988.

[23]Sun, C.-C., and Childs, M. E., "A Modified Wall Wake Velocity Profile for Turbulent Compressible Boundary Layers," *Journal of Aircraft,* Vol. 10, No. 6, 1973, pp. 381–383.

[24]Sturek, W. B., and Danberg, J. E., "Supersonic Turbulent Boundary Layer in Adverse Pressure Gradient. Pt. I: The Experiment," *AIAA Journal,* Vol. 10, No. 4, 1972, pp. 475–480.

[25]Sturek, W. B., and Danberg, J. E., "Supersonic Turbulent Boundary Layer in Adverse Pressure Gradient. Pt. II: Data Analysis," *AIAA Journal,* Vol. 10, No. 5, 1972, pp. 630–635.

[26]Papamoschou, D., and Roshko, A., "Observations of Supersonic Free Shear Layers," AIAA Paper 86-0162, Reno, NV, Jan. 1986.

[27]Etheridge, D. W., and Kemp, P. H., "Measurements of Turbulent Flow Downstream of a Rearward-Facing Step," *Journal of Fluid Mechanics,* Vol. 86, Pt. 3, June 1978, pp. 545–566.

[28]Andreopoulos, J., and Bradshaw, P., "Measurements of Interacting Turbulent Shear Layers in the Near Wake of a Flat Plate," *Journal of Fluid Mechanics,* Vol. 100, Pt. 3, Oct. 1980, pp. 639–668.

[29]Ikawa, H., and Kubota, T., "Investigation of Supersonic Turbulent Mixing Layer with Zero Pressure Gradient," *AIAA Journal,* Vol. 13, No. 5, 1975, pp. 566–572.

[30]Chandrsuda, C., and Bradshaw, P., "Turbulence Structure of a Reattaching Mixing Layer," *Journal of Fluid Mechanics,* Vol. 110, Sept. 1981, pp. 171–194.

[31]Bradshaw, P., and Wong, F. Y. F., "The Reattachment and Relaxation of a Turbulent Shear Layer," *Journal of Fluid Mechanics,* Vol. 52, Pt. 1, March 1972, pp. 113–135.

[32]Eaton, J. K., and Johnston, J. P., "A Review of Research on Subsonic Turbulent Flow Reattachment," *AIAA Journal,* Vol. 19, No. 9, 1981, pp. 1093–1100.

[33]Lee, S. C., and Harsha, P. T., "Use of Turbulent Kinetic Energy in Free Mixing Studies," *AIAA Journal,* Vol. 8, No. 6, 1970, pp. 1026–1032.

[34]Harsha, P. T., and Lee, S. C., "Correlation Between Turbulent Shear Stress and Turbulent Kinetic Energy," *AIAA Journal,* Vol. 8, No. 8, 1970, pp. 1508–1510.

[35]Bradshaw, P., Ferriss, D. H., and Atwell, N. P., "Calculation of Boundary-Layer Development Using the Turbulent Energy Equation," *Journal of Fluid Mechanics,* Vol. 28, Pt. 3, May 1967, pp. 593–616.

[36]Bradshaw, P., and Ferriss, D. H., "Calculation of Boundary-Layer Development Using the Turbulent Energy Equation: Compressible Flow on Adiabatic Walls," *Journal of Fluid Mechanics,* Vol. 46, Pt. 1, March 1971, pp. 83–110.